CRYSTAL GROWTH & DESIGN

pubs.acs.org/crystal

Article

Crystal Growth and Structure–Property Optimization of Thermally Annealed Nanocrystalline Ga_2O_3 Films

Nanthakishore Makeswaran, Anil K. Battu, Eva Deemer, and C. V. Ramana*

Cite This: *Cryst. Growth Des.* 2020, 20, 2893–2903

Read Online

ACCESS | Metrics & More | Article Recommendations

ABSTRACT: The effects of thermal annealing on the crystal chemistry, crystallization process, index of refraction, mechanical properties, and electrical characteristics of nanocrystalline Ga_2O_3 films was evaluated. Ga_2O_3 thin films were sputtered onto Si(100) substrates at 500 °C utilizing a Ga_2O_3 ceramic target, while postdeposition thermal annealing was performed between a range of 500–900 °C. Both structural quality and packing density of the Ga_2O_3 films was improved by the thermal annealing as indicated by the X-ray diffraction and ellipsometry studies. The atomic force microscopy analysis indicates that the annealing temperature has a dramatic effect on surface roughness, especially when the annealing temperature exceeds 700 °C. Corroborating with structure and morphology changes, the high values of hardness and elastic modulus are noted for Ga_2O_3 films annealed at higher temperatures (800–900 °C). Index of refraction (n) and extinction coefficient (k) results, and their dispersion profiles indicate that the annealing temperature strongly influences the optical properties. The refractive index values vary in the range of 1.78–1.84 (632 nm) because of the gradual improvement of structural quality, texturing, and packing density upon thermal annealing. A correlation between annealing temperature, optical characteristics, and electrical characteristics in Ga_2O_3 films is established.

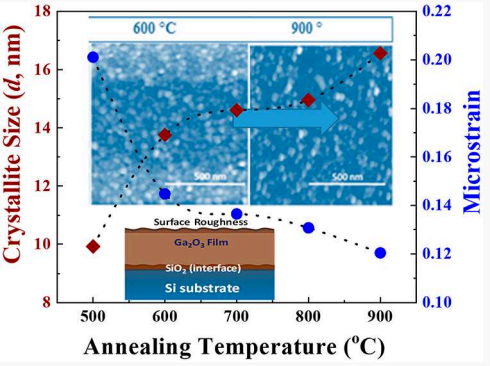

INTRODUCTION

Gallium oxide (Ga_2O_3) is a wide band gap oxide and is potentially applicable in a variety of technological applications ranging from electronics and electrooptics to photonics, catalysts and integrated sensors.[1−12] Ga_2O_3 is the second material with as wide band gap as ∼4.9 eV.[10,14] Ga_2O_3 demonstrates multiple structures, potentially useful material properties, as well as chemical and thermodynamic stability.[4,6,7,10] These properties lend themselves to the application of Ga_2O_3 thin films and nanostructures in numerous fields, such as high-temperature sensors,[8,9] electronics,[10−13] luminescent phosphors, antireflective coatings,[15,16] lithium batteries,[17] and solar cells.[15,16] Additionally, gallium oxide exhibits polymorphism, namely, the α, β, γ, δ, and ε phases of Ga_2O_3 are well-known.[10,18,19] Of particular interest is monoclinic β-Ga_2O_3 which is thermally stable with a predicted high breakdown field strength of 8 MV/cm.[10,18] The high thermal stability of β-Ga_2O_3 is a useful property for the development of high-temperature chemical sensors.[8,9] These types of sensors can be readily used in automotive and power generation industries.[8,9] Ga_2O_3-based materials also exhibit high-temperature stability, coupled with deep ultraviolet transparency, making them candidates for extreme environments chemical sensors and for transparent electrodes in UV optoelectronics, and thin-film transistors.[8,9,20] To utilize this material in these technological applications, the basic understanding of crystallography, surface/interface structure, chemistry and properties, and establishing structure–property relationship are the keys to control the properties and enhance the ultimate device performance of Ga_2O_3 films.

Thermal annealing at the postfabrication stage is common in the utilization of electronic materials for practical device applications.[21−29] Furthermore, it is widely accepted that thermal annealing strongly influences the microstructure and properties of oxide-based electronic materials.[21−25] In fact, a great number of efforts were directed in the literature toward understanding the effect of annealing atmosphere, such as nitrogen or oxygen, and annealing temperature on the physical, mechanical, chemical, and electronic properties of Ga_2O_3 films.[24−30] For instance, semiconductor-to-insulating electronic transformation was reported for Si-doped β-Ga_2O_3 films when annealing was performed at 800–850 °C in O_2 atmosphere.[28] In the majority of previous studies, it was reported that the oxygen vacancy concentration and carrier concentration

Received: August 26, 2019
Revised: March 12, 2020
Published: March 13, 2020

https://dx.doi.org/10.1021/acs.cgd.9b01130
Cryst. Growth Des. 2020, 20, 2893–2903

decrease after thermal annealing of β-Ga_2O_3 single crystals.[24] Note that intrinsic Ga_2O_3 displays *n*-type conductivity while the electrical properties can be tuned by suitable dopants into Ga_2O_3. Metal−organic chemical vapor deposition (MOCVD) Ga_2O_3 films were observed to possess an amorphous-to-crystalline structural transformation with superior crystalline quality and surface smoothness when annealed at 900 °C.[27,29] Because of improved crystalline quality, the annealed MOCVD Ga_2O_3 films also minimized the optical band gap while displaying high transparency.[27,29]

Zhaoqing Feng et al. made use of laser-assisted molecular beam epitaxy (MBE) to deposit β-Ga_2O_3 thin films at 600 °C.[29] The MBE β-Ga_2O_3 epilayers were annealed at varying temperatures durations in air and oxygen.[29] Annealing at 800−900 °C for 30 or 60 min led to the samples becoming close the β-phase Ga_2O_3, while exposure to higher temperature or extended durations led to fully compromised crystal quality.[29] The annealed epilayers experience a red-shift of absorption edge compared to the nonannealed samples, where in-plane compressive strain relaxation during thermal annealing was thought to be the cause of the bandgap differences. The authors also claimed that, after annealing in air and O_2 atmospheres, the nonstoichiometric GaO_x phases are reduced and a full conversion to Ga_2O_3 is experienced, that is accompanied by the oxygen vacancy concentration decrease.[29] High-temperature annealing in the O_2 atmosphere is considered the reason for the larger photocurrent in the oxygen annealed devise as such an atmosphere promotes β-phase Ga_2O_3 recrystallization. The annealing of the β-Ga_2O_3 films grown by anodic oxidation of n-GaAs wafers induces a phase evolution sequence.[26] When annealed in an argon atmosphere at temperatures of 600 and 900 °C, for 30 min, the reaction tendency was observed to be fully different.[26] The gallium oxide films with no thermal treatment react readily with acids confirming the presence of the α-phase.[26] The gallium oxide films annealed at 600 °C dissolved in a hydrochloric acid solution, and the films annealed at 900 °C did not react with the acids.[26] Also, after annealing at 600 and 900 °C, the electrical conductivity of Ga_2O_3 films increased and the voltage growth decreased from 80−90 to 4−6 V.[26] The annealing of pulsed laser deposition (PLD) deposited β-Ga_2O_3 films on (0001) oriented sapphire substrates indicate the films were polycrystalline with preferential orientation along [401].[30] The films were of the same composition, no matter the different temperatures of annealing. The film annealed at 800 °C display greater surface smoothness and comparatively larger crystallite size.[30] The film annealed at 1000 °C show surface lateral feature size enhancement. These films are strain free and have a [40−1] orientation.[30] The high-temperature annealing results in an Al diffusion from the sapphire substrate.[30]

This brief review and analysis of the literature clearly indicates that the structure, morphology, optical, and electrical properties are dependent on the origin of film deposition and conditions employed for annealing. Specifically, it can be conclusively noted that the annealing atmosphere and the annealing temperature, along with the time of annealing strongly influence the crystal structure, texturing, chemical composition, electronic and optical properties, which ultimately decide on the performance the β-Ga_2O_3 films when integrated into device applications. However, most of the previous studies were performed on the Ga_2O_3 single crystals. The information available on the thermal annealing effect on the nanocrystalline β-Ga_2O_3 films is meager. Specifically, the efforts directed and information available on the sputter-deposited nanocrystalline β-Ga_2O_3 films is scanty. Therefore, the purpose of this was work was to understand the effect of thermal annealing on the structural, optical, and electrical properties of sputter-deposited nanocrystalline β-Ga_2O_3 films. The efforts were directed to understand the growth and crystallization behavior and thus to derive enhanced ability for manipulation with the specific crystal structure and phase while optimizing the conditions to obtain desirable properties for the integration of Ga_2O_3 films in electronic device applications. Results are presented and discussed in this article to establish a relation between annealing temperature, crystal structure, crystal growth behavior, optical constants, surface morphology, and electrical characteristics.

EXPERIMENTAL SECTION

Sample Fabrication. Radio-frequency sputtering was used to deposit nanocrystalline Ga_2O_3 films were fabricated on silicon (Si) (100) wafers.[1,31] The deposition procedures and experimental conditions established for the fabrication of amorphous and nanocrystalline Ga_2O_3 films with desired stoichiometry have been reported elsewhere.[1,31] Briefly, and for clarity purpose, the details of the experimental procedures are outlined below. Si(100) substrates were thoroughly cleaned with adopted procedures and finally with dry nitrogen.[1,31] The chamber was subsequently evacuated to a base pressure of $\sim 10^{-6}$ Torr in preparation for deposition. A Ga_2O_3 ceramic target (Plasmaterials, Inc.), of 2 in. diameter and 99.999% purity, was employed for the sputtering.[1,20,31] The Ga_2O_3 target was mounted on a 2 in. sputter gun, located a distance of 7 cm from the substrate. 40 W was initially applied to target during the introduction of high-purity argon (Ar) gas into the chamber to induce plasma ignition. Once a steady plasma stream was achieved, target power was gradually increased to their respective sputtering power for final deposition. Ar and oxygen (O_2) flow rates were controlled via MKS mass flow meters.[1,31] Presputtering was done on the target for 15−20 min with a closed shutter above the gun. A total deposition time of 3 h was kept constant for each samples at sputtering power of 100 W to produce the films. The samples were deposited at substrate temperatures (T_s) 500 °C, the optimum temperature to induce nanocrystalline β-phase Ga_2O_3 films.[1,31] To ensure uniform surface coverage, the substrate was kept constantly rotated during the deposition. Each sample was subsequently annealed for 1 h between 600 and 900 °C in the air.

Characterization. *X-ray Diffraction (XRD).* Grazing incidence X-ray diffraction (GIXRD) was used for crystal structure analysis of the Ga-oxide films. A Bruker D8 Advance device utilizing Cu Kα radiation (λ = 1.54 Å) was used for the room temperature measurements. The grazing incident angle was fixed to 1° for the incoming X-ray beam to focus on studying the surface and layers of the films.[1,20,31] The detector scanned from 10° to 67° at a rate of 0.5 s/step.

Atomic Force Microscopy (AFM). The surface morphology of as-deposited and annealed Ga_2O_3 films was examined utilizing atomic force microscopy (AFM). The experiments were performed to derive the Ga_2O_3 film surface morphology characteristic parameters, namely, the average surface roughness (R_a), root-mean-square roughness (R_q), ten point average roughness (R_Z), and the third highest peak to third lowest valley height (R_{3Zi}).[20,31−33] The details of experimental procedures employed for thin metal/oxide film surface characterization were reported previously.[20,31,33] All the AFM experiments were performed (Ntegra, NT-MDT, UK) in contact mode after double sided tape was employed to mount the samples on sapphire substates. The AFM measurements made use of probes with a 0.01−0.5 N/m force constant (NT-MDT CSG/10). Any actual surface imaging analysis of Ga_2O_3 films was done multiple measurements were taken to ensure the probe tip quality. Tip quality was of particular concern and was qualitatively assessed by examination of the resultant images for clarity and artifact presence. The instrument

https://dx.doi.org/10.1021/acs.cgd.9b01130
Cryst. Growth Des. 2020, 20, 2893−2903

manufacturer supplied standards were employed for calibration. The average surface roughness of the Ga_2O_3 films was calculated using the using[32]

$$R_a = \frac{1}{L}\int_0^L |Z(x)|dx \quad (1)$$

in which $Z(x)$ is the function describing the surface profile analyzed in terms of height and position (Z and x, respectively) over the evaluation length L. Surface roughness, that is, variations in height, is measured either along a single line, or along a set of parallel line profiles. R_a is the arithmetic average of the absolute values of the surface height deviations measured from the mean plane.[31−33] For the this experiment's analysis each 500 nm × 500 nm image has 65 536 sampling points. R_q represents is the standard deviation of the variance from the mean plane from the image sampling points. The symmetry of distribution is characterized by Surface skewness (RSK). Skewness and kurtosis parameters play a vital role in understanding surface characteristics. R_a and R_q are primarily used for classifying surfaces of the same type and that are similarly manufactured.

Nanomechanical Characterization. The hardness (H) and reduced elastic modulus (E_r) were obtained for the as-deposited and annealed Ga_2O_3 films by nanoindentation tests (Hysitron T1750 Tribo nanoindentor). We adopted the procedures established in our laboratory[20,33] combined with standard practices existing in the literature.[34] These approaches are quite successful for determining the H and E_r values of metal and oxide thin films.[33] A triangular pyramid Berkovich diamond indenter with a normal angle of 65.3° between the tip axis and triangular pyramid faces was used for the nanoindentation. The effective size of the apex was approximately 100 nm. The system was set to and automatically performed seven indents[33] on the sample. The indent pattern took the shape of an "H" with three on each side and one central indent. This simple pattern in recommended for indenter tip calibrations, where the "H" pattern will be performed on fused quartz with indents spaced 15 μm apart for low load systems. The load versus displacement curves and indentation patterns are compared with the original probe calibration sheet supplied with each probe. The mechanical characteristics, H and E_r, where calculated using the Oliver and Pharr method[34] with the help of loading and unloading curves. The elastic modulus (E_r) can be calculated by finding the stiffness (S) of the film, using the slope of the unloading curve, via the following relation:[34]

$$E_r = \frac{\sqrt{\pi}}{2}\frac{S}{\sqrt{A}} \quad (2)$$

A is the area of contact at peak load. Hardness is found using the same value for the area of contact along with the maximum load (P_{max}):

$$H = \frac{P_{max}}{A} \quad (3)$$

Determining the maximum indentation depth not in excess of 10% of the total film thickness was done with a series of initial load-controlled indentation tests.[33,34] This is done to avoid the substrate effects[33] and obtain the reliable mechanical properties of Ga-oxide films. Additionally, to account for the statistical data and reliability, a total of 17 indents at a selected load of 250 μN L were performed at 0.2 s^{-1} strain rate, and then, the average H and E_r values were calculated for each sample. The final averaged H and E_r values were considered to further analyze the thin film mechanical behavior.

Scratch Testing. Adhesion to a chosen the substrate is one of the primary characteristics determining the coating quality and life endurance for any nanoscale film or coating.[33] To this end film adhesion was analyzed by nanoscratch testing (Hysitron T1750 Tribo nanoindentor). Testing was performed at room temperature under continuously increasing load increments from 0 to 8000 μN utilizing the same standard triangular pyramid Berkovich diamond indenter tip as the nano indention testing.[33] Total scratch length was 16 μm with a scratch speed was 0.18 μm/s.

Spectroscopic Ellipsometry. Spectroscopic ellipsometry (SE) was used to determine the optical properties as well as the surface/interface characteristics.[20] Δ and ψ were determined over a wavelength range of 200−1600 nm at 300 K in the air using a J. A. Woollam vertical variable-angle spectroscopic ellipsometer in conjunction with a computer controlled Berek wave plate compensator (J.A. Woollam Co, Lincoln, NE). 60°, 65°, and 70° were utilized as the angles of incidence for the measurements.[20] Post analysis of the ellipsometry data performed using commercially available WVASE32 software.[35]

The sample microstructure and optical properties can be related to the SE measured angles as defined by[35−37]

$$\rho = R_p/R_s = \tan\Psi \exp(i\Delta) \quad (4)$$

where R_p is the complex reflection coefficients of the light polarized parallel to the plane of incidence, while R_s is the light perpendicular to the plane.[35−37] The Levenberg−Marquardt regression algorithm was used to minimize the mean-squared error (MSE):[36]

$$\mathrm{MSE} = \frac{1}{2N - M}\sum_{i=1}^{n}\left[\left\{\frac{(\Psi_{exp} - \Psi_{calc})}{\sigma_{\Psi_i}^{exp}}\right\}^2 + \left\{\frac{(\Delta_{exp} - \Delta_{calc})}{\sigma_{\Delta_i}^{exp}}\right\}^2\right] \quad (5)$$

In the formula, Ψ_{exp}, Ψ_{calc} and Δ_{exp}, Δ_{calc} are the measured and calculated ellipsometry functions.[36] N represents number of measured Ψ, Δ pairs, while the number of fitted parameters in the optical model is given by M, and finally, σ represents the standard deviations of the data points.[36] Also, to account for the optical inhomogeneity, multiple measurements and analyses were made to determine the degree of inhomogeneity in these oxide films deposited by sputtering. We used the standard procedures established and the variation in index of refraction reported is $\Delta n = \pm 0.01$.

Electrical Characteristics. Resistivity of the samples was measured using the four-point Van der Pauw method. This made use of four electrical contacts on the sample constructed with a two part conducting epoxy and silver wires.[38] Eight different combinations of the four contact points on the sample were used to find voltage and current, that is, in the first set of measurements, current is applied to one arbitrarily chosen pair of electrodes and voltage is measured across the remaining two electrodes with the process being repeated for other contact configurations.[38] A Keithley 220 programmable current source supplying a current of 2 mA was used. To measure the voltage, a Keithley 196 sensitive digital voltmeter was used, while a 196 DMM system was used to read the intervening currents.[38] To switch between contacts a Keithley 2001 switch. A LABVIEW data acquisition system via the IEEE-488 GPIB for automatic data recording was used to take data from the respective meters.[38] The Van der Pauw principle, which takes into account the sample thickness, the shape factor, and other limitations, was used to determine the final resistivity.[38]

RESULTS AND DISCUSSION

Surface Morphology. The AFM patterns of as-deposited and annealed Ga_2O_3 films are shown in Figures 1−3. Figure 1 depicts topographic images of the thin films morphology while the corresponding grain area analysis is illustrated in Figure 2. The surface roughness and grain histograms are shown in Figure 3, respectively. The morphology of the nanoparticulate film surfaces for as-deposited Ga_2O_3 films demonstrate conically shaped grains distributed uniformly over the film surface of the intrinsic Ga_2O_3 films while the root-mean-square surface roughness value was ∼1 nm. These reported AFM values for intrinsic Ga_2O_3 films are in excellent agreement with those reported in the literature.[38,39] It is clear from results presented here that increasing the annealing temperature produces substantial changes in the surface morphology of the Ga_2O_3 films. The increasing grain size and surface roughness values of the Ga_2O_3 films exhibit a clear dependence on the annealing temperature (Figure 3). Also, as noted in Figure 3a,

https://dx.doi.org/10.1021/acs.cgd.9b01130
Cryst. Growth Des. 2020, 20, 2893−2903

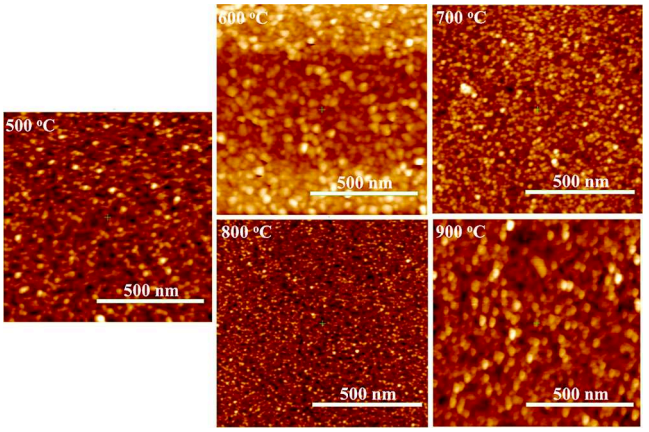

Figure 1. AFM morphology micrographs of Ga_2O_3 films as a function of annealing temperature.

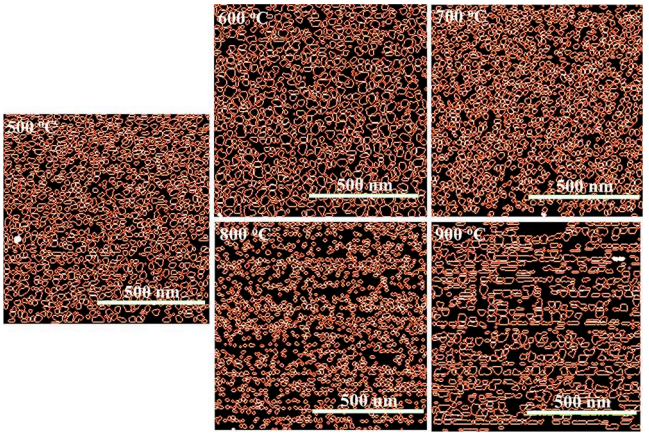

Figure 2. AFM grain analysis micrographs of Ga_2O_3 films as a function of annealing temperature.

the average roughness (R_a) is well correlated with the root mean square (R_q). The surface roughness increases with increasing temperature until a temperature of 800 °C, and at this point, there is a large decrease in surface roughness. One can see from the grain area histogram (Figure 3b) that, between 700 and 800 °C, there are competitive bimodal phases contributed to grains of different areas in contrast to grain analysis on as-deposited films and those annealed at the highest annealing temperature (900 °C), where a much more consistent distribution of grains appears. The single numerical parameters, R_a and R_q, are useful to classify the same type of surfaces which have been produced using the same method. The annealing temperature has a dramatic effect on surface roughness, especially when the annealing temperature exceeds 700 °C. While these results agree, in general, with results reported in literature for Ga_2O_3 films fabricated by physical methods, differences arise due to the differences in synthesis conditions adopted for deposition, substrate materials, and physical parameters (thickness, density, etc.). For instance, while the noted trend is very similar to annealing behavior of polycrystalline Ga_2O_3 films made by anodic oxidation of n-GaAs wafers,[26] there are significant difference in the observed values of roughness values and grain size and shapes. The Ga_2O_3 anodic films exhibit linear grain sizes, where grains were in the form of squares with a side length of 600−700 nm.[26] After annealing, Ga_2O_3 anodic film roughness increased to 100−120 nm, which exceedingly higher compared to sputter-deposited films. While the trend is similar, the differences are primarily attributed to the preparation methods, that is, anodic oxidation under oxygen plasma versus sputter deposition under reactive conditions. The later results in more finer grains while Ga_2O_3 anodic films tend to result in larger or microsize grains rather than nanoscale dimensions. On the other hand, our results closely agree with those reported for Ga_2O_3 films made by pulsed laser deposition. Similar to sputter-deposited Ga_2O_3 films, PLD Ga_2O_3 films were also of the same composition, no matter the different temperatures of annealing.[30] The PLD Ga_2O_3 films annealed at 800 °C exhibit a smoother surface and relatively larger feature size.[30] Similar to PLD Ga_2O_3 films, the sputter-deposited films also attain the maximum grain size and lower surface roughness for annealing at 800−900 °C.

Crystal Chemistry, Crystal Growth, and Mechanism. Figure 4a shows the GIXRD patterns for the both the as-deposited and annealed Ga_2O_3 films. The results indicate annealing temperatures play a substantial role in determining crystal structure. The as-deposited nanocrystalline Ga_2O_3 sample corresponds to the monoclinic β-phase (space group $C2/m$). The XRD peaks, due to diffraction from crystal planes of (−201), (400), (002), and (−204), which correlate to 2θ values of 18.95, 30.05, 31.74, and 64.17, in accordance with JCPDS (00-043-1012).[1] Significant changes are not visible in the XRD patterns until temperatures of 700 °C. The peaks become shaper with an intensity increase in addition to the appearance of (104), (113), and (−211) peaks. This

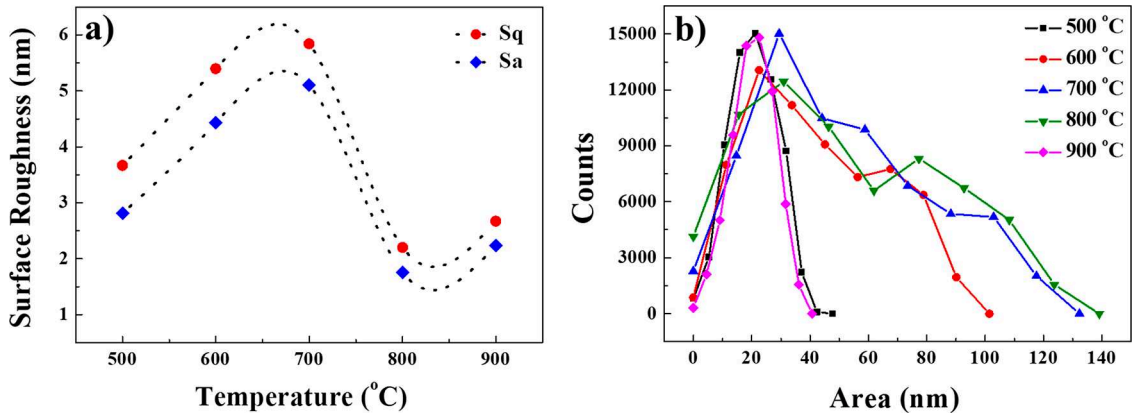

Figure 3. AFM surface roughness analysis and correlation between roughness and temperature (a) and grain analysis histograms (b).

https://dx.doi.org/10.1021/acs.cgd.9b01130
Cryst. Growth Des. 2020, 20, 2893−2903

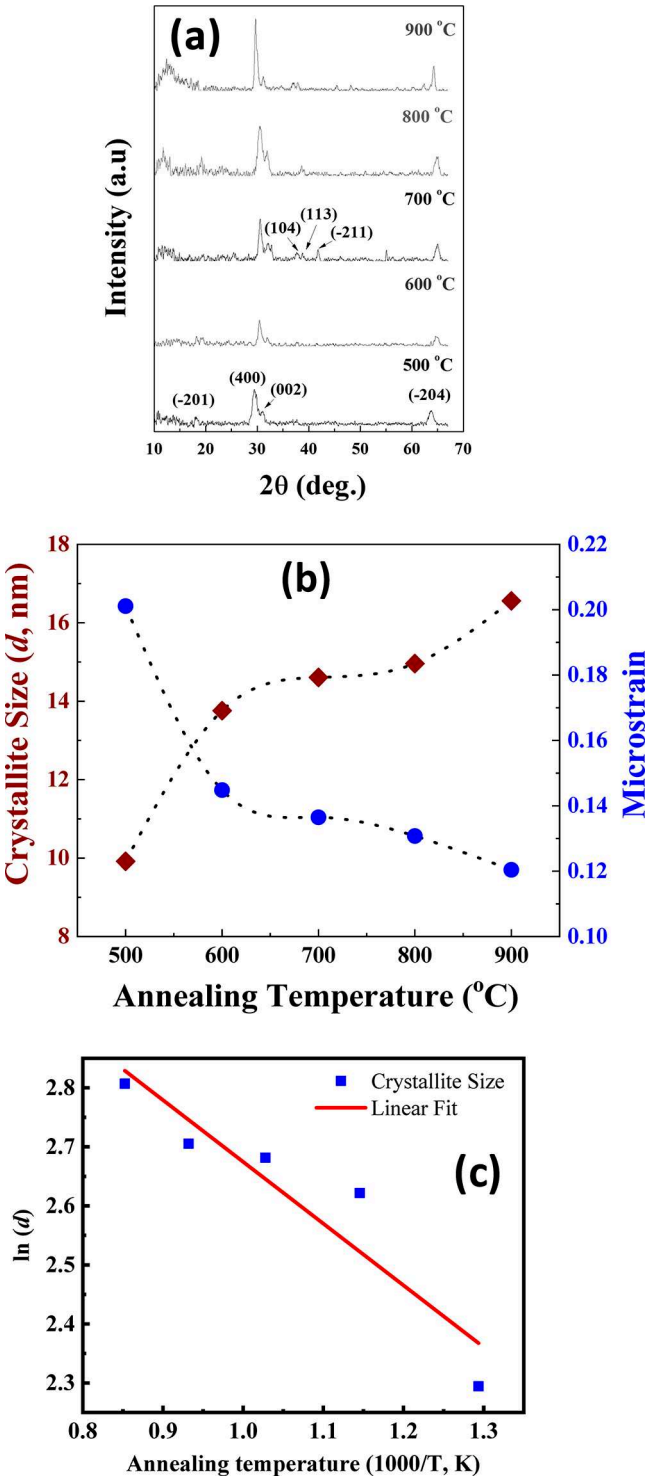

Figure 4. (a) XRD patterns of as-deposited and annealed Ga_2O_3 films. (b) Variation of crystallite size and microstrain in the Ga_2O_3 films. (c) Arrhenius plot of crystallite size versus temperature.

observation indicates the thermally induced crystallization leading to further structural evolution in the sputter-deposited Ga_2O_3 films. Further increase in the annealing temperature to 900 °C induces texturing of the Ga_2O_3 films, as can be seen in XRD data (Figure 4a). The peak intensity for (400) and (−201) reflections increases with thermal annealing indicating the preferential growth or texturing of the Ga_2O_3 films. Specifically, the (400) peak intensity increases considerably while the peak becomes narrower with a noticeable reduction in full width at half-maximum (fwhm) indicating a higher crystallinity. The results are in general agreement with those reported for MOCVD Ga-oxide films.[25,27,29] Those samples exhibited an amorphous-to-crystalline structural transformation with improved crystalline quality and a smoother surface structure with an annealing temperature of 900 °C.[25,27] Similarly, under thermal annealing, PLD β-Ga_2O_3 films on sapphire substrates also exhibited the typical behavior of polycrystalline nature and texturing upon annealing at temperatures of 800−1000 °C, although annealing at the high end of this temperature range resulted in Al diffusion from the substrate.[30] Thus, from the results presented in this work, in conjunction with previous results available in the literature, it can be conclusively stated that the thermal annealing at higher temperatures 800−900 °C induces crystallization and introduces changes in the crystallite size and morphology.

To understand the effect of thermal annealing on crystallinity and crystal growth, the average crystallite size of the sputter-deposited nanocrystalline Ga_2O_3 films is calculated using the Scherrer's equation[40]

$$d = \frac{0.9\lambda}{\beta \cos\theta} \tag{6}$$

where d represents the average crystallite size, the angle of the peak is θ, λ is the wavelength of X-rays, and β is the width of the peak at its half intensity. The intense (400) peak data was used for calculations. Similarly, determining the microstrain in the Ga_2O_3 films is made by further analysis of the XRD data. The origin of the microstrain is related to the lattice misfit, which, in turn, depends upon the fabrication parameters. The microstrain is calculated using the relation:[40]

$$\varepsilon = \frac{\beta \cos\theta}{4} \tag{7}$$

In this equation β once again is the full width at half-maximum while θ is instead the Bragg angle. The variation of the average crystallite size and microstrain with annealing temperature is shown in Figure 4b. The average crystallite size increases from 10 to 16 (±1) nm with the increase of temperature from 500 to 900 °C. The nature of annealing, crystallization (explained in XRD) and grain growth mechanism plays a critical role for the change in the average crystallite size. The decrease in the strain values implies that the films becoming strain free and thermal annealing improves the crystalline nature of the Ga_2O_3 films.

Finally, to understand the fundamental mechanism of crystallization and growth behavior in nanocrystalline Ga_2O_3 films under the effect of increasing thermal annealing temperature, the data obtained from XRD and AFM were analyzed in terms of simple models available in the literature. Temperature, a key thermodynamic parameter, plays an major role in deciding the microstructure and properties of thin films produced by the physical or chemical deposition methods.[20,41,42] Usually, when the effect of temperature is not sufficient to produce, amorphous films are the result, while increasing annealing temperature or time of annealing can induce sufficient atom mobility and, hence, crystallization in the films.[41−45] From XRD and AFM data analyses, it can be observed that the increasing annealing temperature improves crystallization and induces texturing. As the average crystallite size and morphology changes, the enlarged grain-size, in

https://dx.doi.org/10.1021/acs.cgd.9b01130
Cryst. Growth Des. 2020, 20, 2893−2903

addition to their distribution characteristics, a direct result of further increase in annealing temperature, can only be due to restructuring of the Ga_2O_3 films on the Si(100) substrate. The crystallite size data were analyzed and fit to the Arrhenius relation, similar to diffusion coefficient in solid-state materials and phenomena, where the crystallite-size (d) typically depend on temperature as[46]

$$d = d_o \exp(-\Delta E/k_B T) \quad (8)$$

where ΔE is the activation energy, k_B is the Boltzmann constant, T is the absolute temperature, and d_0 is a pre-exponential factor that depends on the physical properties of the substrate-oxide film configuration. If it is assumed that the crystallite-size relates directly to surface diffusion and atom rearrangement, it can be expected to witness the increase in d with annealing temperature in accordance with the Arrhenius relation. As such, the d-values, determined from XRD, were fitted in Figure 4c, where it is evident that the experimental data fits to the first order exponential growth function. All the data fits to an exponential function (Figure 4c). This feature indicates the thermally activated mechanism as operative in the crystallization, which account for the changes in the Ga_2O_3 film's surface morphology and average crystallite size as a function of annealing temperature, as seen in the data from AFM and XRD measurements. Figure 4c displays the Arrhenius plots for the XRD data. The data are well fitted by a linear function. An activation energy of 0.12 (±0.01) eV for the nanocrystalline, monoclinic β-Ga_2O_3 was determined from the slope of the linear plot. Directly comparing this value with other reports is not currently possible as there is no available data for nanocrystalline Ga_2O_3 films, whether deposited by sputtering or other physical/chemical vapor deposition methods. This value (0.12 eV), while small, is to be expected for nanocrystalline films with the given size parameters, particularly when compared to the data of some other micro- and nanocrystalline metal-oxide thin films, such as monoclinic HfO_2 films[47] and nanocrystalline, tetragonal WO_3 films.[42,46]

Mechanical Properties. One of the key components of structure optimization for thin films lies with tailoring their mechanical properties.[20,33] These properties, in turn, can be governed by various parameters, such as the coating-substrate hardness relation, film thickness, or roughness of the film, while the reactions are based largely on the rate of application and magnitude of stress.[45,46] Large stresses may present in thin films that can lead to their deformations and cracking, and understanding and minimizing these stresses, how they occur, and in what ways they influence film integrity is vital in thin film production.[48,49] A key component of determining overall wear resistance of thin films lies with elastic modulus and its relation to elastic strain to failure, which in turn is related to the hardness/elastic modulus (H/E).[49−51] These parameters were determined using the indentation load versus depth characteristics of as-deposited and annealed Ga_2O_3 films presented in Figure 5. Note that the mechanical properties of the films are strongly influenced by the underlying substrate material's properties.[33] Therefore, penetration depth characteristics as a function of applied indentation load become critical to find the optimum load and proceed further with other measurements. As shown in Figure 5, the applied indentation load is varied from 100 to 2000 μN, while recording the corresponding penetration depth at each and every applied load. At the initial applied load of 100 μN, the penetration depth is 9 nm for the as-deposited Ga_2O_3 film. The penetration depth increases with increasing applied indentation load. For as-deposited Ga_2O_3 film, at the applied load of 350 μN, the total penetration depth is as high as reaches to 19 ± 1 nm, which nearly reaches 10% of total film thickness. Thus, this load has been considered to be optimum for testing all of the as-deposited and annealed Ga_2O_3 films for better comparison of nanomechanical properties. In general, to obtain reliable and true information on the films, the penetration depth must not exceed 10% of total film thickness.[20,33] Thus, all samples readily satisfy this requirement. However, while the indentation depth for the annealed Ga_2O_3 films at different temperatures is almost same, minimal differences (±5 nm) in penetration depth is due to variation in the structural quality of the respective films with steadily increasing annealing temperatures.

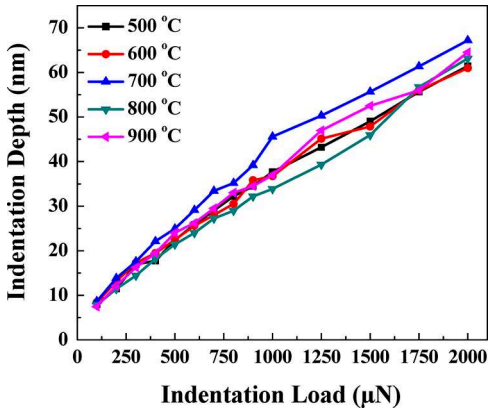

Figure 5. Applied indentation load versus indentation depth characteristics of Ga_2O_3 thin films. The data shown are for samples annealed under variable temperatures.

The loading and unloading curves for Ga_2O_3 thin films are shown in Figure 6a. The data is obtained with an indentation load of 350 μN. It can be noted that the load versus displacement curves are slightly different for Ga_2O_3 films annealed at different temperatures. Close inspection of the data indicates a slight shift with increasing annealing temperature, especially for Ga_2O_3 thin films annealed at 700−900 °C. These data enable us to determine the hardness (H) and elastic modulus (E_r) of the Ga_2O_3 thin films. The variation of H and E_r values with annealing temperature of Ga_2O_3 films are presented in Figure 6b and 6c, respectively. There was a noticeable difference in the H and E_r values for the Ga_2O_3 films annealed at different temperatures. The observed differences can be attributed mainly to the variation of crystallinity and morphology of Ga_2O_3 films as a function of annealing temperature. It can be noted (Figure 6c) that the H value of 27 GPa decreases initially for the Ga_2O_3 films annealed at 700 °C. This may be due to the residual stress relaxation by thermal annealing. However, it can be noted that further increase in annealing temperature to 800 °C increases the H values to ∼30 GPa, and the level remains more or less constant with further increase in the annealing temperature to 900 °C. The crystal structure improvement of Ga_2O_3 films with increasing annealing temperature accounts for the increased H values at >700 °C. Thus, the results indicated that the hardness of the annealed Ga_2O_3 films is predominantly due to the crystallization upon thermal annealing, as revealed by both XRD and AFM analyses.

https://dx.doi.org/10.1021/acs.cgd.9b01130
Cryst. Growth Des. 2020, 20, 2893−2903

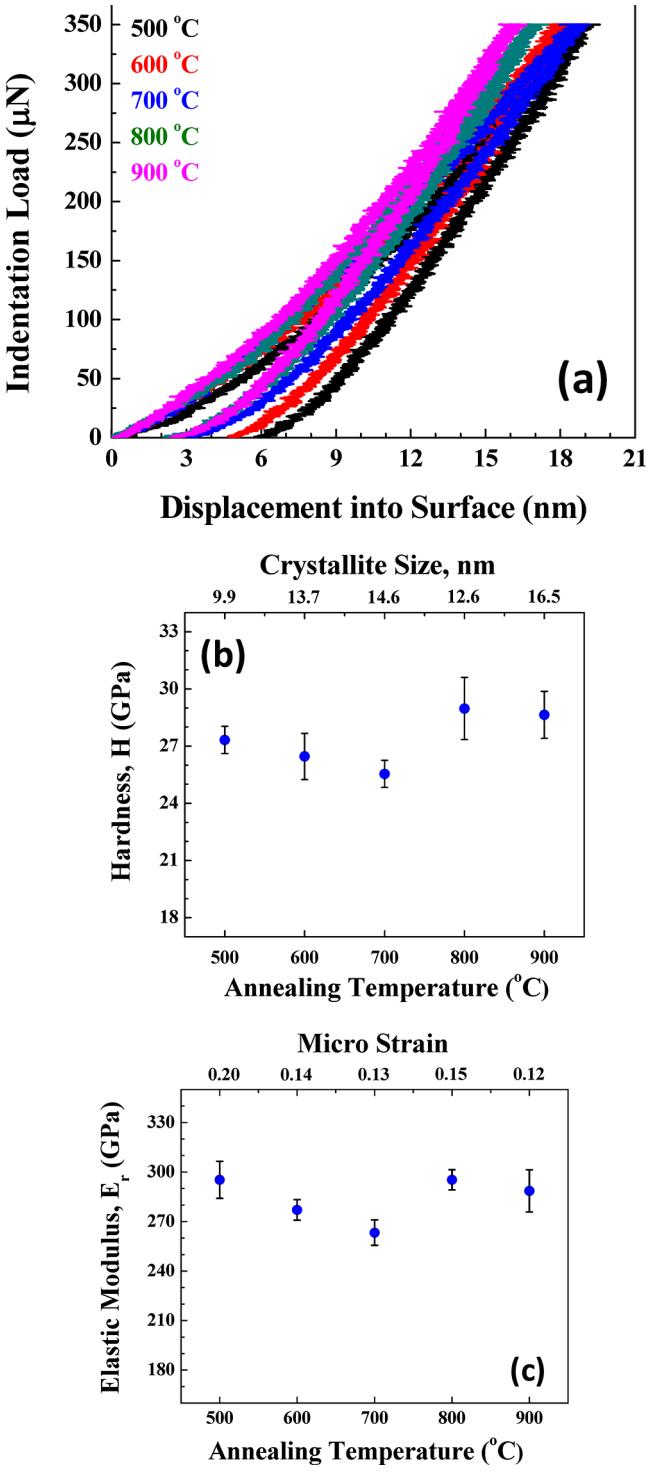

Figure 6. (a) Load versus displacement curves obtained for Ga_2O_3 films. (b) Hardness values of Ga_2O_3 films. (c) Elastic modulus of Ga_2O_3 films.

In Figure 6c, the variation in E_r of Ga_2O_3 thin films is shown as a function of annealing temperature. The trend is very similar to the H results shown in Figure 6b. The elastic modulus represents the resistance to small changes in separation of adjacent atoms in relation to interatomic bonding forces. The magnitude of the elastic modulus depends on the slope of the load−displacement curve. The E_r values for the film deposited at 500 °C is ∼295 GPa, and with the annealing effect, E_r values decreased to ∼265 GPa for the film annealed at 700 °C. On further temperature increasing, the E_r values increased to ∼295 GPa for the films annealed at 800 and 900 °C. Overall, there was not a noticeable change in elastic modulus values.

The nanoscratch results of as-deposited and annealed Ga_2O_3 films are shown in Figure 7. In Figure 7a, the images of 20 μm × 20 μm are shown, as obtained before and after the scratch text of the Ga_2O_3 films, while the corresponding depth profiles are shown in Figure 7b. The Ga_2O_3 films exhibit no indication of delamination from the substrate. The nanoscratch testing was conducted in such a way that the only area immediately surrounding the scratch deforms, whereas the remaining part of the film is undamaged. The scratch test was conducted in ramping mode,[33] in which normal force is increased with direction of tip travel. The depth profile characteristic for the as-deposited Ga_2O_3 film is ∼67 nm after the nanoscratch. On the other hand, for the film annealed at 900 °C, the depth is only about 53 nm. The data clearly indicate that there is no significant change in the early stages of annealing, while significant changes occur as discussed in XRD and nanomechanical sections. The main observation is that, while scratch tests revealed material pile-up, there was no evidence of delamination of the as-deposited and annealed Ga_2O_3 films.

Optical Constants and Electrical Resistivity. The spectroscopic ellipsometry measurements and analyses were employed to determine the optical constants of the Ga_2O_3 films. The refractive index (n) and extinction coefficient (k) were fitted with Cauchy dispersion model,[52−54] which is quite successful in evaluating the optical properties of Ga_2O_3 films made by several deposition methods. This model was chosen partly due to transparency in respective wavelength regions for Ga_2O_3 films and partly due to it providing a successful fit to the data and serving to explain the optical properties of the films.[20,38] The Cauchy equation for refractive index n as a function of wavelength λ is

$$n(\lambda) = A + B/\lambda^2 + C/\lambda^4 \quad (9)$$

where A, B, and C are the Cauchy coefficients that are unique to a given material. The three constants play dominant roles $n(\lambda)$ along different wavelengths with A for long wavelengths, B for wavelengths in the middle of the visible spectrum, and C for shorter wavelengths. However, extracting meaningful physical information from ellipsometry requires forming an optical model of the sample, accounting for several distinct layers with varying optical dispersions.[53,54] The layer interfaces act as optical boundaries where light is refracted and reflected per the Fresnel relations. Figure 8 shows the stack model used to determine the optical constants of the Ga_2O_3 films. From the top down the model contains: Ga_2O_3 film, $Ga_2O_3/SiO_2/Si$ interface and Si substrate. To accurately fit the data both surface and interface roughness were also considered.

Figure 8 shows the spectral dependencies of ellipsometric parameters Ψ (azimuth) and Δ (phase change); these parameters are fitted using appropriate models to determine film thickness and the optical constants, refractive index (n) and extinction coefficient (k). These determinations are derived from the best fit between experimental and simulated spectra. The curves obtained for annealed Ga_2O_3 films indicate, as shown in Figure 9, agreement between the experimental and simulated data for the entire annealing temperature range.

https://dx.doi.org/10.1021/acs.cgd.9b01130
Cryst. Growth Des. 2020, 20, 2893−2903

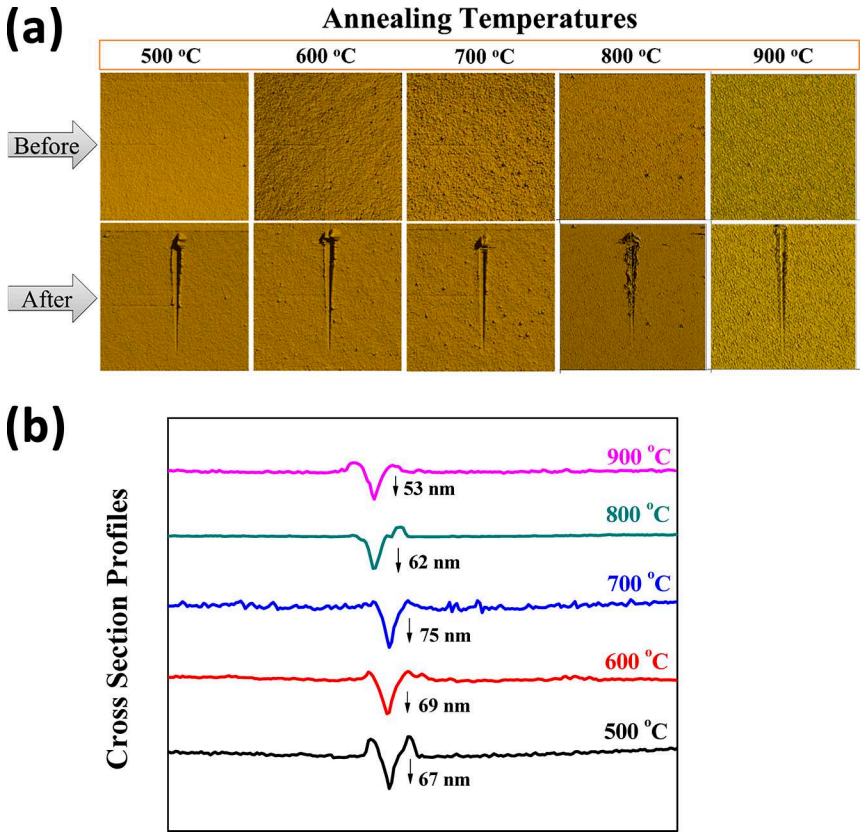

Figure 7. (a) Scratch testing data of Ga_2O_3 thin films. The images represent before and after the scratch test performed on the samples. (b) Scratch testing profiled of Ga_2O_3 thin films. The depth decreases with increasing annealing temperature can be attributed to the improved crystallinity.

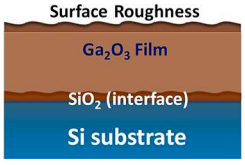

Figure 8. Stack model of the GTO sample constructed for ellipsometry data analysis.

The dispersion refractive index profiles determined from SE data for Ga_2O_3 films are shown in Figure 10. There is a sharp increase of fundamental absorption of energy across the band gap correlating to shorter wavelengths. The thermal-annealing induced changes in structure and the dependence on annealing temperature are clear in the dispersion curves (Figure 10). The data reveals that there is a progressive increase in n values with increasing annealing temperature. Throughout the spectrum the extinction coefficient values are low and very close to zero. An understanding of the structural quality of Ga_2O_3 films can also be derived from the dispersion profiles of $n(\lambda)$. Specifically, the curves (Figure 10) indicate the increasing tendency of n value of the Ga_2O_3 films which is due to improved crystallinity of the samples. However, we believe that the changes in optical properties and electrical properties are primarily due to changes in the physical characteristics and crystallization but not at all due to any chemical changes.[55] For instance, the spectroscopic analyses on these Ga_2O_3 films as function annealing temperature indicate that the chemical stoichiometry is well maintained in the entire range of T_a. As reported elsewhere, (Ga^{3+}), the highest chemical oxidation state for gallium, exists in both the as-deposited and annealed Ga_2O_3 films.[55] The electronic structure was not observed to have changed significantly, particularly when considering the chemical valence of Ga ions and Ga−O bonds as a function of the thermal annealing.[55] Therefore, the observed trend in optical and electrical properties of in this work attributed to the crystallization and improved packing density of the Ga_2O_3 films upon thermal annealing.

The electrical properties of Ga_2O_3 films as a function of annealing temperature corroborated with the changes in structure and morphology. The Ga_2O_3 thin films deposited at 500 °C had electrical resistivity of 104×10^3 Ω cm, and it slightly increased to 127×10^3 Ω cm for the Ga_2O_3 films annealed at 600 °C. Then it starts decreasing to 85×10^3 Ω cm and significantly down to 1.04×10^2 Ω cm for the Ga_2O_3 films annealed at 800 and 900 °C, respectively. The effect of annealing on the microstructure evident in the electrical resistivity of the Ga_2O_3 films. The electrical resistivity usually becomes higher with grain size reduction usually leads to an increase in electrical resistivity due to the increasing grain boundary volume and associated charge carrier flow impedance.[38,41] Grain boundary scattering becomes a dominant effect leading to higher electrical resistivity as a result of crystallite size becoming smaller than the electron mean free path. Lattice imperfections such as vacancies and dislocations, often present in nanocrystalline materials, also strongly influence electrical resistivity.[38,41] Additionally, lattice strain and associated distortions can negatively affect the charge mobility leading to a decrease in conductivity. The room-temperature electrical resistivity variations with annealing temperature observed for Ga_2O_3 films can be explained taking these factors into consideration. The resistivity decrease by

https://dx.doi.org/10.1021/acs.cgd.9b01130
Cryst. Growth Des. 2020, 20, 2893−2903

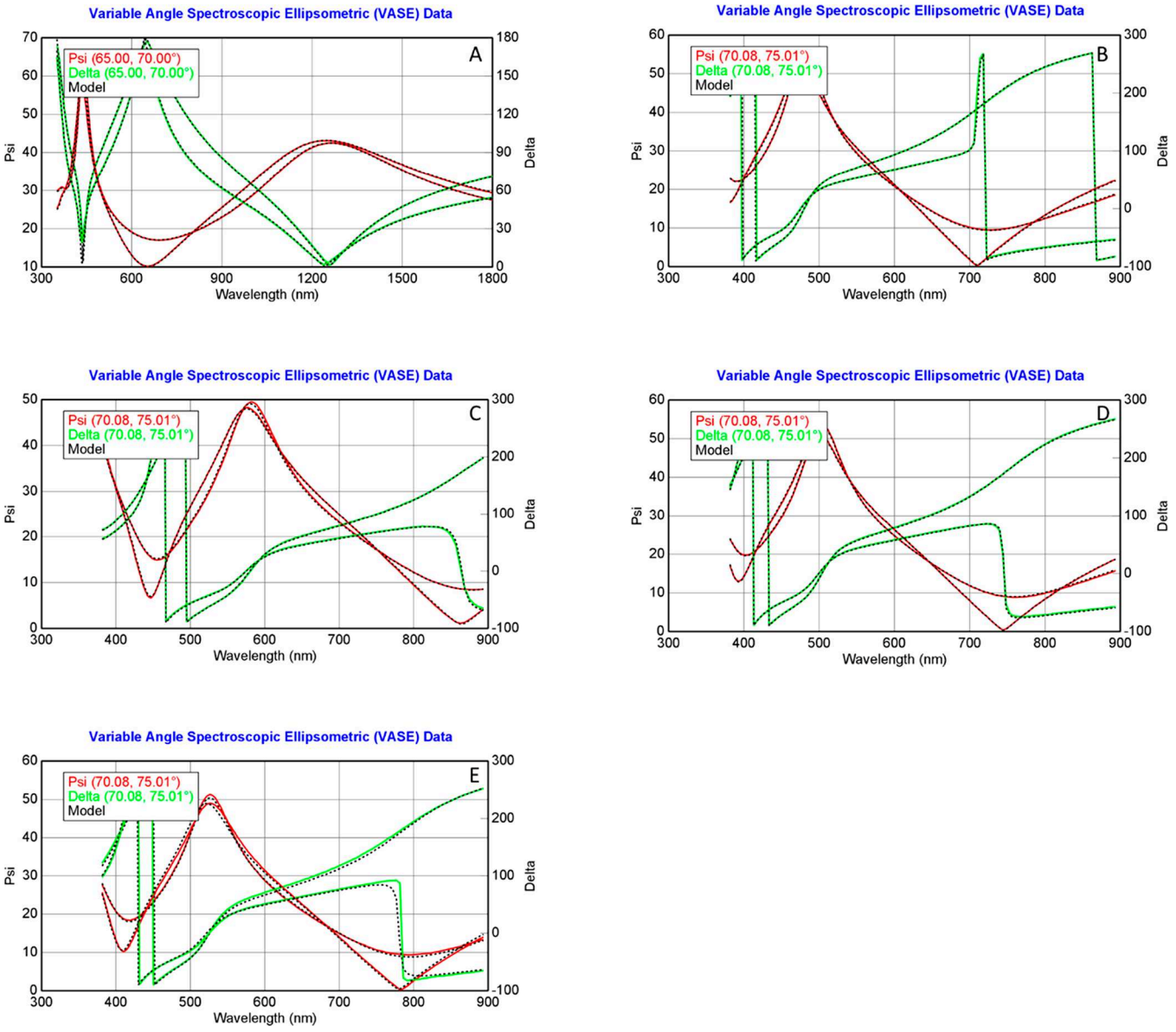

Figure 9. Experimental and modeled curves of Ψ and Δ for gallium oxide films: (A) 500, (B) 600, (C) 700, (D) 800, and (E) 900 °C.

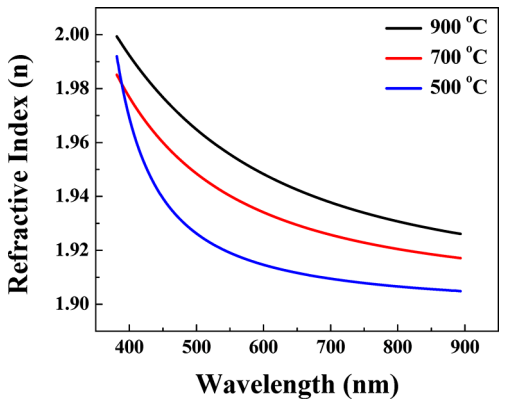

Figure 10. Refractive index profiles of Ga_2O_3 films.

increasing annealing temperature can be attributed to increased crystallinity of the films, as well as a combined effect of the average crystallite size increase and surface morphology variation. This trend in resistivity can then be directly attributed to better crystallinity, larger grains, and fewer grain boundaries in the samples annealed at higher temperatures.

SUMMARY AND CONCLUSIONS

The effect of post-deposition thermal annealing on the crystallization or growth process, crystal chemistry, mechanical properties, refraction index profiles, and electrical characteristics of sputter-deposited, nanocrystalline Ga_2O_3 films has been evaluated. It can be concluded that annealing plays a major role in altering the structure and morphology of the Ga_2O_3 films. The thermal annealing to 800−900 °C improves the structural quality and packing density of the Ga_2O_3 films. While the films annealed at intermediate temperatures (up to 700 °C) become exceedingly rough, Ga_2O_3 films annealed at 800−900 °C exhibit relatively smoother morphology, distribution characteristics and optical quality. The refraction index values at 632 nm increase from 1.78 to 1.84 that corroborates with gradual improvement of structural quality, texturing, and packing density upon thermal annealing at 800−

https://dx.doi.org/10.1021/acs.cgd.9b01130
Cryst. Growth Des. 2020, 20, 2893−2903

900 °C. The correlation established between annealing temperature and optical and electrical characteristics in Ga_2O_3 films may useful and can serve as foundation nanocrystalline Ga_2O_3 films for application in sensors and optical and optoelectronic devices.

AUTHOR INFORMATION

Corresponding Author

C. V. Ramana − *Center for Advanced Materials Research (CMR), University of Texas at El Paso, El Paso, Texas 79968, United States;* orcid.org/0000-0002-5286-3065; Email: rvchintalapalle@utep.edu

Authors

Nanthakishore Makeswaran − *Center for Advanced Materials Research (CMR), University of Texas at El Paso, El Paso, Texas 79968, United States*

Anil K. Battu − *Center for Advanced Materials Research (CMR), University of Texas at El Paso, El Paso, Texas 79968, United States*

Eva Deemer − *Center for Advanced Materials Research (CMR), University of Texas at El Paso, El Paso, Texas 79968, United States;* orcid.org/0000-0001-9112-8971

Complete contact information is available at: https://pubs.acs.org/10.1021/acs.cgd.9b01130

Notes

Any opinions, findings, and conclusions or recommendations expressed in this material are those of the authors and do not necessarily reflect the views of the United States Air Force. The authors declare no competing financial interest.

ACKNOWLEDGMENTS

The authors acknowledge, with pleasure, support from the National Science Foundation (NSF) with NSF-PREM Grant DMR-1827745. This material is also based upon work supported by the Air Force Office of Scientific Research under award number FA9550-18-1-0387.

REFERENCES

(1) Kumar, S. S.; Rubio, E.; Noor-A-Alam, M.; Martinez, G.; Manandhar, S.; Shutthanandan, V.; Thevuthasan, S.; Ramana, C. V. Structure, Morphology, and Optical Properties Of Amorphous And Nanocrystalline Gallium Oxide Thin Films. *J. Phys. Chem. C* **2013**, *117*, 4194−4200.

(2) Zhang, W.; Naidu, B. S.; Ou, J. Z.; O'Mullane, A. P.; Chrimes, A. F.; Carey, B. J.; Wang, Y.; Tang, S. Y.; Sivan, V.; Mitchell, A.; Bhargava, S. K.; Kalantar-zadeh, K. Liquid Metal/Metal Oxide Frameworks with Incorporated Ga_2O_3 for Photocatalysis. *ACS Appl. Mater. Interfaces* **2015**, *7*, 1943−1948.

(3) Mu, W.; Jia, Z.; Cittadino, G.; Yin, Y.; Luperini, C.; Hu, Q.; Li, Y.; Zhang, J.; Tonelli, M.; Tao, X. Ti-Doped β-Ga_2O_3: A Promising Material for Ultrafast and Tunable Lasers. *Cryst. Growth Des.* **2018**, *18*, 3037−3043.

(4) Zade, V.; Mallesham, B.; Shantha-Kumar, S.; Bronson, A.; Ramana, C. V. Interplay between Solubility Limit, Structure, and Optical Properties of Tungsten-Doped Ga_2O_3 Compounds Synthesized by a Two-Step Calcination Process. *Inorg. Chem.* **2019**, *58*, 3707−3716.

(5) Mazeina, L.; Picard, Y. N.; Maximenko, S. I.; Perkins, F. K.; Glaser, E. R.; Twigg, M. E.; Freitas, J. A., Jr.; Prokes, S. M. Growth of Sn-Doped β-Ga_2O_3 Nanowires and Ga_2O_3−SnO_2 Heterostructures for Gas Sensing Applications. *Cryst. Growth Des.* **2009**, *9*, 4471−4479.

(6) Rafique, S.; Han, L.; Zorman, C. A.; Zhao, H. Synthesis of Wide Bandgap β-Ga_2O_3 Rods on 3C-SiC-on-Si. *Cryst. Growth Des.* **2016**, *16*, 511−517.

(7) Sun, H.; Li, K.-H.; Torres Castanedo, C. G.; Okur, S.; Tompa, G. S.; Salagaj, T.; Lopatin, S.; Genovese, A.; Li, X. HCl Flow-Induced Phase Change of α-, β-, and ε-Ga_2O_3 Films Grown by MOCVD. *Cryst. Growth Des.* **2018**, *18*, 2370−2376.

(8) Bartic, M.; Baban, C. I.; Suzuki, H.; Ogita, M.; Isai, M. β-Gallium Oxide as Oxygen Gas Sensors at a High Temperature. *J. Am. Ceram. Soc.* **2007**, *90*, 2879−2884.

(9) Ogita, M.; Higo, K.; Nakanishi, Y.; Hatanaka, Y. Ga_2O_3 Thin Film for Oxygen Sensor at High Temperature. *Appl. Surf. Sci.* **2001**, *175*, 721−725.

(10) Pearton, S. J.; Yang, J.; Cary, P. H.; Ren, F.; Kim, J.; Tadjer, J. M.; Mastro, M. A. A Review of Ga_2O_3 Materials, Processing, and Devices. *Appl. Phys. Rev.* **2018**, *5*, 011301−011356.

(11) Yang, G.; Jang, S.; Ren, F.; Pearton, S. J.; Kim, J. Influence of High-Energy Proton Irradiation on β-Ga_2O_3 Nanobelt Field-Effect Transistors. *ACS Appl. Mater. Interfaces* **2017**, *9*, 40471−40476.

(12) Jamison, J. S.; May, B. J.; Chien, S.-C.; McComb, D. W.; Grassman, T. J.; Windl, W.; Myers, R. C.; et al. Ferromagnetic Epitaxial μ-Fe_2O_3 on β-Ga_2O_3: A New Monoclinic Form of Fe_2O_3. *Cryst. Growth Des.* **2019**, *19*, 4205−4211.

(13) Chen, Y.; Xia, X.; Liang, H.; Abbas, Q.; Liu, Y.; Du, G. Growth Pressure Controlled Nucleation Epitaxy of Pure Phase ε- and β-Ga_2O_3 Films on Al_2O_3 via Metal−Organic Chemical Vapor Deposition. *Cryst. Growth Des.* **2018**, *18*, 1147−1154.

(14) Peelaers, H.; Van de Walle, C. G. Brillouin Zone and Band Structure of β-Ga_2O_3. *Phys. Status Solidi B* **2015**, *252*, 828−832.

(15) Tomm, Y.; Ko, J.; Yoshikawa, A.; Fukuda, T. Floating zone growth of β-Ga_2O_3: a new window material for optoelectronic device applications. *Sol. Energy Mater. Sol. Cells* **2001**, *66*, 369−374.

(16) Zhang, Y.; Yan, J.; Li, Q.; Qu, C.; Zhang, L.; Xie, W. Optical and Structural Properties of Cu-doped β-Ga_2O_3 films. *Mater. Sci. Eng., B* **2011**, *176*, 846−849.

(17) Patil, S. B.; Kim, I. Y.; Gunjakar, J. L.; Oh, S. M.; Eom, T.; Kim, H.; Hwang, S.-J. Phase Tuning of Nanostructured Gallium Oxide via Hybridization with Reduced Graphene Oxide for Superior Anode Performance in Li-Ion Battery: An Experimental and Theoretical Study. *ACS Appl. Mater. Interfaces* **2015**, *7*, 18679−18688.

(18) He, H.; Orlando, R.; Blanco, M. A.; Pandey, R.; Amzallag, E.; Baraille, I.; Rérat, M. First-principles study of the structural, electronic, and optical properties of Ga_2O_3 in its monoclinic and hexagonal phases. *Phys. Rev. B: Condens. Matter Mater. Phys.* **2006**, *74*, 195123.

(19) Yoshioka, S.; Hayashi, H.; Kuwabara, A.; Oba, F.; Matsunaga, K.; Tanaka, I. Structures and energetics of Ga_2O_3 polymorphs. *J. Phys.: Condens. Matter* **2007**, *19*, 346211.

(20) Ramana, C. V. Properties of Sputter-Deposited Gallium Oxide. In *Gallium Oxide*; Elsevier, 2019; pp 47−66.

(21) Irfan, I.; Gao, Y. Effects of Exposure and Air Annealing on MoO_x Thin Films. *J. Photonics Energy* **2012**, *2*, 021213.

(22) Kim, C.-K.; Kim, E.; Lee, M. K.; Park, J.-Y.; Seol, M.-L.; Bae, H.; Bang, T.; Jeon, S.-B.; Jun, S.; Park, S.-h. K.; Choi, K. C.; Choi, Y.-K. An Electro-thermal annealing (ETA) Method to Enhance the Electrical Performance of Amorphous-Oxide-Semiconductor (AOS) Thin-Film Transistors (TFTs). *ACS Appl. Mater. Interfaces* **2016**, *8*, 23820−23826.

(23) Ke, W.; Zhao, D.; Cimaroli, A. J.; Grice, C. R.; Qin, P.; Liu, Q.; Xiong, L.; Yan, Y.; Fang, G. Effects of Annealing Temperature of Tin Oxide Electron Selective Layers on The Performance of Perovskite Solar Cells. *J. Mater. Chem. A* **2015**, *3*, 24163−24168.

(24) Son, N. T.; Goto, K.; Nomura, K.; Thieu, Q. T.; Togashi, R.; Murakami, H.; Kumagai, Y.; Kuramata, A.; Higashiwaki, M.; Koukitu, A.; Yamakoshi, S.; Monemar, B.; Janzén, E. Electronic Properties of the Residual Donor in Unintentionally Doped β-Ga_2O_3. *J. Appl. Phys.* **2016**, *120*, 235703.

(25) Cao, Q.; He, L.; Feng, X.; Xiao, H.; Ma, J. Effect of Annealing on the Structural and Optical Properties of β-Ga_2O_3 Films Prepared

on Gadolinium Gallium Garnet (110) by MOCVD. *Ceram. Int.* **2018**, *44*, 830−835.
(26) Kalygina, V. M.; Zarubin, A. N.; Nayden, Ye. P.; Novikov, V. A.; Petrova, Yu. S.; Tolbanov, O. P.; Tyazhev, A. V.; Yaskevich, T. M. The Effect of Annealing on the Properties of Ga_2O_3 Anodic Films. *Semiconductors* **2012**, *46*, 267−273.
(27) Kim, H. W.; Kim, N. H. Annealing Effects on the Properties of β-Ga_2O_3 Thin Films Grown on Sapphire by Metal Organic Chemical Vapor Deposition. *Appl. Surf. Sci.* **2004**, *230*, 301−306.
(28) Gogova, D.; Wagner, G.; Baldini, M.; Schmidbauer, M.; Irmscher, K.; Schewski, R.; Galazka, Z.; et al. Structural Properties of Si-doped β-Ga_2O_3 Layers Grown by MOVPE. *J. Cryst. Growth* **2014**, *401*, 665−669.
(29) Feng, Z.; Huang, L.; Feng, Q.; Li, X.; Zhang, H.; Tang, W.; Zhang, J.; Hao, Y. Influence of Annealing Atmosphere on the Performance of a β-Ga_2O_3 Thin Film and Photodetector. *Opt. Mater. Express* **2018**, *8*, 2229.
(30) Goyal, A.; Yadav, B. S.; Thakur, O. P.; Kapoor, A. K.; Muralidharan, R. Effect of Annealing on β-Ga_2O_3 Thin Film Grown by Pulsed Laser Deposition Technique. *J. Alloys Compd.* **2014**, *583*, 214−219.
(31) Rubio, E. J.; Mates, T. E.; Manandhar, S.; Nandasiri, M.; Shutthanandan, V.; Ramana, C. V. Tungsten Incorporation into Gallium Oxide: Crystal Structure, Surface and Interface Chemistry, Thermal Stability, and Interdiffusion. *J. Phys. Chem. C* **2016**, *120*, 26720−26735.
(32) De Oliveira, R.; Albuquerque, D.; Cruz, T.; Yamaji, F.; Leite, F. Measurement of the Nanoscale Roughness by Atomic Force Microscopy: Basic Principles and Applications. *In. Technol.* **2012**, 147.
(33) Battu, A. K.; Zade, V. B.; Deemer, E.; Ramana, C. V. Microstructure-Mechanical Property Correlation in Size Controlled Nanocrystalline Molybdenum Films. *Adv. Eng. Mater.* **2018**, *20*, 1800496.
(34) Oliver, W. C.; Pharr, G. W. An Improved Technique for Determining Hardness and Elastic Modulus using Load and Displacement Sensing Indentation Experiments. *J. Mater. Res.* **1992**, *7*, 1564−1583.
(35) Woollam, J. A. *Guide to Using WVASE32 Spectroscopic Ellipsomtry Data Acquisition and Analysis Software*; JA Woollam Co, Inc., 2005.
(36) Jellison, G. E. The Calculation of Thin Film Parameters From Spectroscopic Ellipsometry Data. *Thin Solid Films* **1996**, *290−291*, 40−45.
(37) Fujiwara, H. *Spectroscopic Ellipsometry: Principles and Applications*; John Wiley & Sons, 2007.
(38) Ramana, C. V.; Rubio, E.; Barraza, C.; Miranda Gallardo, A.; McPeak, S.; Kotru, S.; Grant, J. Chemical Bonding, Optical Constants, and Electrical Resistivity of Sputter-Deposited Gallium Oxide Thin Films. *J. Appl. Phys.* **2014**, *115*, 043508.
(39) Leedy, K. D.; Chabak, K. D.; Vasilyev, V.; Look, D. C.; Boeckl, J. J.; Brown, J. L.; Tetlak, S. E.; Green, A. J.; et al. Highly Conductive Homoepitaxial Si-doped Ga_2O_3 Films on (010) β-Ga_2O_3 by Pulsed Laser Deposition. *Appl. Phys. Lett.* **2017**, *111*, 012103.
(40) Williamson, G. K.; Hall, W. H. Discussion of the Theories of Line Broadening. *Acta Metall.* **1953**, *1*, 22−31.
(41) Vemuri, R.S.; Bharathi, K. K.; Gullapalli, S.K.; Ramana, C.V. Effect of structure and size on the electrical properties of nanocrystalline WO_3 films. *ACS Appl. Mater. Interfaces* **2010**, *2*, 2623−2627.
(42) Kalidindi, N. R.; Manciu, F. S.; Ramana, C. V. Crystal Structure, Phase, and Electrical Conductivity of Nanocrystalline $W_{0.95}Ti_{0.05}O_3$ Thin Films. *ACS Appl. Mater. Interfaces* **2011**, *3*, 863−868.
(43) Shvets, V. A.; Aliev, V. Sh; Gritsenko, D. V.; Shaimeev, S. S.; Fedosenko, E. V.; Rykhlitski, S. V.; Atuchin, V. V.; Gritenko, V. A.; Taplin, V. M.; Wong, H.; et al. Electronic Structure and Charge Transport Properties of Amorphous Ta_2O_5 films. *J. Non-Cryst. Solids* **2008**, *354*, 3025−3033.
(44) Mudavakkat, V. H.; Atuchin, V. V.; Kruchinin, V. N.; Kayani, A.; Ramana, C. V. Strtucture, Morphology and Optical Properties of Nanocrystalline Yttrium Oxide (Y_2O_3) Thin Films. *Opt. Mater.* **2012**, *34*, 893−900.
(45) Atuchin, V. V.; Lebedev, M. S.; Korolkov, I. V.; Kruchinin, V. N.; Maksimovskii, E. A.; Trubin, S. V. Composition-Sensitve Growth Kinetics and Dispersive Optical Properties of Thin $Hf_xTi_{1-x}O_2$ ($0 \leq x \leq 1$) Films Prepared by the ALD Method. *J. Mater. Sci.: Mater. Electron.* **2019**, *30*, 812−823.
(46) Kittel, C. *Introduction to Solid State Physics*; Wiley: New York, 1968.
(47) Ramana, C. V.; Kamala Bharathi, K.; Garcia, A.; Campbell, A. L. Growth Behavior, Lattice Expansion, Strain and Surface Morphology of Nanocrystalline, Monoclinic HfO_2 Thin Films. *J. Phys. Chem. C* **2012**, *116*, 9955−9960.
(48) Holmberg, K.; Ronkainen, H.; Matthews, A. Tribology of Thin Coatings. *Ceram. Int.* **2000**, *26*, 787−795.
(49) Nix, W. D. Mechanical Properties of Thin Films. *Metall. Trans. A* **1989**, *20*, 2217.
(50) Beake, B. D.; Vishnyakov, V. M.; Valizadeh, R.; Colligon, J. S. Influence of Mechanical Properties on the Nanoscratch Behaviour of Hard Nanocomposite TiN/Si_3N_4 Coatings on Si. *J. Phys. D: Appl. Phys.* **2006**, *39*, 1392−1397.
(51) Leyland, A.; Matthews, A. On the Significance of the H/E Ratio in Wear Control: a Nanocomposite Coating Approach to Optimised Tribological Behaviour. *Wear* **2000**, *246*, 1−11.
(52) Jenkins, F. A.; White, H. E. *Fundamentals of Optics*, 4th ed.; McGraw-Hill, Inc., 1981.
(53) Ramana, C. V.; Mudavakkat, V. H.; Kamala Bharathi, K.; Atuchin, V. V.; Pokrovsky, L. D.; Kruchinin, V. N. Enhanced Optical Constants of Nanocrystalline Yttrium Oxide Films. *Appl. Phys. Lett.* **2011**, *98*, 031905.
(54) Atuchin, V. V.; Kalinkin, A. V.; Kochubey, V. A.; Kruchinin, V. N.; Vemuri, R. S.; Ramana, C. V. Spectroscopic Ellipsomtery and X-Ray Photoelectron Spectroscopy of La_2O_3 Thin Films Deposited by Reactive Magnetron Sputtering. *J. Vac. Sci. Technol., A* **2011**, *29*, 021004.
(55) Makeswaran, N.; Battu, A. K.; Swadipta, R.; Manciu, F. S.; Ramana, C. V. Spectroscopic Characterization of Electronic Structure, Chemical Bonding, and Band Gap in Thermally Annealed Polycrystalline Ga_2O_3 Thin Films. *ECS J. Solid State Sci. Technol.* **2019**, *8*, Q3249−Q3253.

https://dx.doi.org/10.1021/acs.cgd.9b01130
Cryst. Growth Des. 2020, 20, 2893−2903